A Modeling Study of the Causes and Predictability of the Spring 2011 Extreme US Weather Activity

Siegfried Schubert[1], Yehui Chang[2], Hailan Wang[3], Randal Koster and Max Suarez

Global Modeling and Assimilation Office

NASA GSFC, Greenbelt, Maryland

Revised

8 May 2016

Submitted to

Journal of Climate

[1] Corresponding author address: Siegfried Schubert, 8800 Greenbelt Rd., NASA/GSFC, Greenbelt, MD 20771. E-mail: siegfried.d.schubert@nasa.gov

[2] Also, Goddard Earth Sciences Technology and Research (GESTAR), Morgan State University, Baltimore, Maryland

[3] Also, Science Systems and Applications, Inc., Lanham, Maryland

Abstract

This study examines the causes and predictability of the spring 2011 U.S. extreme weather using the Modern-Era Retrospective analysis for Research and Applications (MERRA) reanalyses and Goddard Earth Observing System, version 5 (GEOS-5) Atmospheric General Circulation Model simulations. The focus is on assessing the impact on precipitation of sea surface temperature (SST) anomalies, land conditions, and large-scale atmospheric modes of variability. A key result is that the April record-breaking precipitation in the Ohio River Valley was primarily the result of the unforced development of a positive North Atlantic Oscillation (NAO)-like mode of variability with unusually large amplitude, limiting the predictability of the precipitation in that region at one month leads. SST forcing (La Nina conditions) contributed to the broader continental scale pattern of precipitation anomalies, producing drying in the southern plains and weak wet anomalies in the northeast, while the impact of realistic initial North American land conditions was to enhance precipitation in the upper Midwest and produce deficits in the southeast. It was further found that:

- The March 1 atmospheric initial condition was the primary source of the *ensemble mean precipitation* response over the eastern U.S. in April (well beyond the limit of weather predictability) suggesting an influence on the initial state of the previous SST forcing and/or tropospheric/stratospheric coupling linked to an unusually persistent and cold polar vortex.
- Stationary wave model experiments suggest that the SST-forced base state for April enhanced the amplitude of the NAO response compared to that of the climatological state, though the impact is modest and can be of either sign.

1. Introduction

According to Karl et al. (2011), "*The spring (March-May) of 2011, particularly April, brought extreme weather and climate events to many parts of the United States. Tornadoes, flooding, drought, and wildfires ravaged many parts of the country during the period, and each of these extremes broke long-standing records and have been compared to the 'worst such cases' in history*." Much of the Ohio River Valley in particular experienced historic rainfall amounts during April, with 2011 ranked as the wettest on record (http://www.ncdc.noaa.gov/monitoring-content/sotc/national/statewidepcpnrank/statewidepcpnrank-201104.gif)

As a first step in assessing the causes of such extremes, a preliminary NOAA assessment of the climate factors contributing to the 2011 tornado outbreak (http://www.esrl.noaa.gov/psd/csi/events/2011/tornadoes/) notes that the April 2011 period of very active severe weather occurred during a La Niña event and that, despite the fact that the La Niña event was then in its waning phase, it was still able to affect U.S. weather patterns..

Hoerling et al. (2013a) found that the record 2011 flooding of the Missouri River Basin resulted from a combination of factors: antecedent wet conditions that preconditioned the upper basin toward greater runoff efficiency, a cold and wet 2010-2011 winter with unusually high snow pack, and heavy rains in late spring (likely the most critical factor). They found a modest contribution of SST forcing to the heavy rains, concluding that they were a highly unlikely occurrence driven by random atmospheric variation.

59

60 The above-normal April precipitation across the northern half of the country was juxtaposed with
61 near- to below-average precipitation in the Southern Plains and Southeast. In fact, by the end of
62 April 2011, much of Texas was experiencing extreme-to-exceptional drought conditions
63 (http://droughtmonitor.unl.edu/Home.aspx). While the drought is not the focus of this study, we
64 note that several studies have shown an important link between this drought and the evolving La
65 Nina conditions (e.g., Hoerling et al. 2013b; Seager et al. 2014; Wang et al.2014). The Wang et
66 al. 2014 study in particular highlighted the importance of the tropical Pacific SST during spring
67 2011 in producing a warming and drying tendency in the southern United States, though the
68 amplitude of the response was weaker than observed.

69

70 In the present study we examine the causes and predictability of the springtime 2011 extreme
71 weather activity with a focus on the record-breaking precipitation that occurred in the central and
72 eastern U.S. during April using high-resolution simulations with the NASA GEOS-5
73 Atmospheric General Circulation Model (AGCM). We complement the modeling results with
74 diagnostics derived from NASA's Modern-Era Retrospective Analysis for Research and
75 Applications (MERRA) reanalysis data and a stationary wave model (SWM). Section 2
76 describes the AGCM, the simulations, the MERRA data, and the SWM. Results are presented in
77 Section 3, and Section 4 provides a summary and conclusions.

78

79 **2. The Experiments and Data**

We base part of our analysis on the MERRA reanalysis (Rienecker et al. 2011). MERRA was produced with the NASA GMAO atmospheric data assimilation system (ADAS), which consists of the Goddard Earth Observing System Version 5 (GEOS-5) AGCM (Reinecker et al. 2008; Molod et al. 2015) along with the Grid point Statistical Interpolation (GSI) analysis (Wu et al. 2002; Kleist et al. 2009), which is jointly developed by the GMAO and the National Centers for Environmental Prediction (NCEP). MERRA was run at a resolution of ½° latitude × 2/3° longitude, with 72 vertical levels extending to 0.01hPa. More information about MERRA can be found at: http://gmao.gsfc.nasa.gov/research/merra/. We also make use of the CPC unified gauge-based 0.25° analysis of daily US precipitation (Chen et al. 2008).

Our main results, however, are based on high-resolution runs with the GEOS-5 AGCM (Rienecker et al., 2008; Molod et al. 2015). The model employs the finite-volume dynamics of Lin (2004) and various physics packages (Bacmeister et al., 2006) integrated together using the Earth System Modeling Framework (Collins et al., 2005) – packages such as the Catchment Land Surface Model (Koster et al., 2000) and a modified form of the Relaxed Arakawa-Schubert convection scheme (Moorthi and Suarez 1992). For our experiments, the model (with internal designation Fortuna 2.4) was run with 72 hybrid-sigma vertical levels extending to 0.01hPa and with a ¼° horizontal resolution on a cubed sphere.

Table 1 lists the complete set of simulations. All simulations were initialized on March 1 and integrated through the end of May. The primary set of runs (A) consists of 44 hindcasts for spring 2011 forced with observed SST. All atmospheric and land initial conditions were taken

from MERRA and thus are deemed reasonably realistic. In order to compute anomalies for 2011, we establish a climatology consisting of 6 ensemble members per year covering the period 2000-2010, These runs are treated identically to those for 2011 in that they are forced by observed SST and initialized from MERRA (differing only in the number of ensemble members per year). For convenience we shall refer to that set of runs as (Ac). The anomalies for 2011 were accordingly computed by subtracting out the mean of the Ac runs.

Supplemental series of simulations utilized, for practical reasons, a reduced set of (22) ensemble members. The first supplemental set used climatological SSTs (B and Bc) but the same atmospheric and land initializations as in Series A; thus, by comparing Series A and B, we can assess the impact of the global SST field on the simulated weather. The second supplement set (C) utilized observed SSTs in the tropical Pacific (east of 180°; 20°S to 30°N) and climatological SSTs elsewhere, allowing us, by comparing Series B and C, to isolate the impact of SST in that region. A final supplemental set (D) utilized observed 2011 SST as in (A) but used, over much of North America (130°W-60°W; 35°N-70°N), a set of initial conditions for land states (including soil moisture, soil temperature, and snow) that contain no useful information for the forecasts. In essence, the initial land states for (D) in this region were obtained from states occurring during the previous 11 years: of the 22 ensemble members, two used land states from 1 March 2000, two used land states from 1 March 2001, and so on. Comparing series (A) and (D) thus allows us to assess the impact of the 2011 spring land conditions on weather.

123 The various ensemble members were generated by perturbing the atmospheric state. The
124 perturbations were computed as scaled differences (+/- (x-y)/8) between two arbitrary November
125 atmospheric states (x,y) taken 1 day apart. The somewhat arbitrary scaling factor of 1/8 was
126 chosen simply in an attempt to produce perturbations that are of a size not inconsistent with
127 initial errors typically found in numerical weather prediction. The November-based
128 perturbations were imposed on March 1 atmospheric states; these perturbations were small
129 enough to ensure that the March 1 atmospheric initialization remained climatologically sensible[4].

130

131 We also make use of a stationary wave model (SWM, Ting and Yu 1998) to help diagnose the
132 forcing of the NAO. (The specific SWM experiments we run are described in Section 3.4). The
133 SWM is based on the 3-dimensional primitive equations in σ coordinates and is nonlinear and
134 time-dependent. Model-generated transient disturbances are suppressed by strong damping. The
135 model has rhomboidal wavenumber-30 truncation in the horizontal and 14 unevenly spaced σ
136 levels in the vertical (R30L14). The SWM has been shown to be a valuable tool for diagnosing
137 the maintenance of both climatological and anomalous atmospheric circulation patterns by
138 evaluating the relative roles of stationary wave forcings over specific regions (e.g., Held et al.

[4] Further details of the perturbations are as follows. Only the atmospheric states were perturbed. For experiment A, 44 unique perturbations were produce as describe above, based on 22 pairs of atmospheric states, and both adding and subtracting the scaled difference fields. For Ac, a subset of 6 of the experiment A perturbations were used: the same 6 perturbations were used for each year (2000-2010). Similarly for experiment Bc, a subset of two of the experiment A perturbations were used, and these were repeated for each year (2000-2010). For experiments B and D, the 22 perturbations are a subset of the 44 perturbations used in experiment A

2002; Schubert et al 2011). More details regarding the SWM can be found in Ting and Yu (1998).

3. Results

We begin in section 3.1 with a look at the observations as represented by MERRA data. We focus here on April, the spring month most dominated by extremes. We follow this in Sections 3.2 and 3.3 with an analysis of our AGCM experiments, focusing respectively on simulated ensemble means and intra-ensemble variances. Section 3.4 examines in more detail the role of the NAO.

3.1 Observations (MERRA)

Figure 1 (top left panel) shows that the Northern Hemisphere upper level (250mb) height field during April 2011 was dominated by a positive NAO-like anomaly[5], with large negative anomalies spanning much of northern North America and the North Atlantic. Positive anomalies extend across the southern tier of the U.S. and across parts of Europe and Asia. This pattern is associated with positive zonal wind anomalies (Fig. 1, bottom left panel) that extend from the North Pacific across the United States. The bottom right panel of Figure 1 shows the daily meridional wind variability at upper levels (a measure of storm intensity, e.g., Chang and Fu

[5] The amplitude of the NAO was in fact the largest on record for April, based on the values of the NAO index tabulated by NOAA's Climate Prediction Center (CPC) for the period 1950 - present. Their NAO index is based on a Rotated Principal Component Analysis of the 700mb height field (Barnston and Livezey 1987) http://www.cpc.ncep.noaa.gov/products/precip/CWlink/pna/norm.nao.monthly.b5001.current.ascii.table

157 2002). The variability is enhanced over much of the United States between 30°N and 50°N, as
158 well as upstream over the North Pacific (centered on 30°N), with reduced variability to the north
159 and south of these regions. The precipitation anomalies (Fig. 1, top right panel) highlight the
160 aforementioned record values over the Ohio River basin, with dry conditions over the southern
161 plains and parts of the southeast. The juxtaposition of the positive precipitation anomalies over
162 much of the Ohio River Basin and the enhanced storminess is not surprising in view of the strong
163 link between middle latitude cyclones and extreme precipitation events found in this region for
164 the cold season (e.g., Pfahl and Wernli 2012).

165

166 In order to put these results in a historical perspective, we examine the leading modes of
167 variability of the height field at 250mb during boreal spring (March-May) over the last three
168 decades (1979-2012) using a rotated empirical orthogonal function (REOF; Richman 1986)
169 decomposition. Figure 2 (top left panel) shows that the third leading REOF resembles the NAO
170 pattern and has much in common with the April height anomalies shown in Figure 1 (top left
171 panel). The first and second REOFs (not shown) consist of patterns resembling the Northern
172 Annular Mode (NAM) and the PNA, respectively. We will come back to the role of the NAM in
173 the next section. The monthly time series (rotated principal component or RPC) of REOF 3
174 further emphasizes the dominance of this mode during April of 2011, showing that during this
175 month it attained its largest positive value over the 34-year time span, consistent with the
176 NOAA/CPC results mentioned above. Composites of the precipitation (Fig. 2 top right panel)
177 and daily 250mb meridional wind variance (Fig. 2 bottom right panel) based on the extremes of

178 that RPC further reinforce the importance of this mode for producing anomalous precipitation
179 and weather variability over the eastern United States (cf. Fig. 1).

180

181 *3.2 The Ensemble Mean (forced) Response*

182 The spring 2011 SST anomalies computed with respect to a climatology spanning the years
183 2000-2010[6] (Figure 3) reflect decaying La Nina conditions with the cold eastern tropical Pacific
184 anomalies weakening and the pattern resembling a negative Pacific Decadal Oscillation (PDO).
185 During March and April much of the eastern tropical Pacific is characterized by negative
186 anomalies less than -½°C, with the largest negative values (south of the equator) exceeding
187 1.5°C in magnitude. By May, the eastern equatorial Pacific SST anomalies are nearly zero,
188 while weak cold anomalies remain to the south and over the far eastern North Pacific, with
189 positive anomalies occurring just to the west in the central North Pacific. Also seen are cold
190 conditions over the North Atlantic, some positive anomalies over the tropical Atlantic, and
191 negative anomalies over the Indian Ocean just south of the equator.

192

193 Figure 4 shows the March through May 2011 evolution of precipitation and 2-meter air
194 temperature (T2m) anomalies over North America from MERRA and from the ensemble mean
195 of the model simulations (A-Ac, labeled 'hindcasts'; see Table 1). We note that in these and the
196 following comparisons between model results and observations we always use the same

[6] We note that the SST anomalies with respect to the 2000-2010 climatology (shown in Figure 3) are overall quite similar to those based on a longer climatology (e.g., 1981-2010).

197 climatology (the period 2000-2010) to compute the anomalies. The simulations successfully
198 capture some of the main features of the observed (MERRA) precipitation anomalies, including
199 the positive anomalies over the eastern United States during March and April, though with
200 reduced amplitude, especially during April – the month when the largest anomalies occurred.
201 They also capture the dry conditions over the southern plains and the southeast. The ensemble
202 mean May precipitation anomalies are very diffuse but do show some resemblance to the
203 observations. The spatial correlations over the U.S. (between 25°N-55°N) between the ensemble
204 mean and observed precipitation anomalies are 0.72, 0.51, and 0.28 for March, April and May,
205 respectively. The simulated T2m anomalies also show a considerable resemblance to the
206 observations, with cold anomalies over much of Canada and the northern tier of states and with
207 warm anomalies to the south, especially over the southern plains. The successful simulation of
208 the north/south temperature gradient over the U.S. during April is particularly noteworthy for our
209 study, though the simulated (ensemble mean) gradient is weaker than observed. The month of
210 May shows a transition in the observed (MERRA) T2M pattern, with the cold anomalies more
211 confined to the west – a feature not well captured by the simulations. Nevertheless, the model
212 does an overall better job of reproducing the observed T2M anomaly patterns (compared with
213 those for precipitation). This is reflected in the spatial correlations over the U.S. (between 25°N-
214 55°N) between the ensemble mean and observed T2M anomalies, which are 0.83, 0.78, and 0.53
215 for March, April and May, respectively.

216

217 Figure 5 shows the ensemble mean 250mb height anomalies (top panel) and the 250mb daily
218 meridional wind variance (v'^2, bottom panel) for April. Clearly, some of the key features of the

observations are reproduced in the simulations, including the negative height anomalies over northern North America and the positive anomalies across the southern tier of states though again with reduced amplitude compared to the observations. These anomalies over North America should however not be interpreted as being part of the NAO pattern which has the largest negative anomalies centered further to the east (cf. Figure 2). The pattern of anomalous storminess (as measured by v'^2) across the North Pacific and North America is well reproduced, though also with weaker amplitude. The wave pattern in the height field across Eurasia (Figure 1) is not reproduced in the simulations, suggesting that this feature is not forced by SST.

The ability of the model to reproduce some of the key features of the precipitation, T2M, 250mb height, and v'^2 fields associated with the unusual weather activity over the U.S. during spring 2011 gives us confidence that we can use the model to isolate the sources of the observed changes. Of course, as we have seen, the ensemble mean model response does not reproduce the observed anomalies exactly – something that we should not expect even for a perfect model. In particular, the model does not reproduce the NAO-character of the observed anomalies (it places the negative height anomalies further west and they are overall weaker). This suggests that there is a significant unforced component to the observed anomalies. We will return to that issue in the next section.

We examine now, using the supplemental simulations listed in Table 1 (see Section 2), the separate impacts of SST and land conditions on precipitation (Fig. 6). To help in the interpretation of the results we present in Fig. 7 the corresponding changes in the 250mb height

241 field. The first column of Figure 6 shows that the impact of the global SST forcing (A-B) is
242 primarily to force dry conditions over the southern plains and parts of Mexico, consistent with
243 previous studies (e.g., Seager et al. 2014; Wang et al. 2014). The corresponding height
244 anomalies (first column in Fig. 7) show a wave response during March and April that is typical
245 for La Nina conditions. The key feature during these months is the ridge over the southwest and
246 south central part of the US that tends to block storms approaching from the west leading to the
247 dry conditions in the southern plains as seen in Figure 6. The ridge is presumably also associated
248 with subsidence, further contributing to the drying in that region. In May, the impact of the SST
249 is different, producing a tendency for wet conditions over the northern plains and parts of
250 southern Canada, consistent with the development of an anomalous trough covering much of the
251 continental United States and southern Canada.

252

253 The second column of Figure 6 shows the precipitation anomalies obtained when the observed
254 SSTs are confined to the tropical Pacific (C-B). The anomalies are quite similar to those
255 obtained with the global SST forcing. This is reflected in the spatial correlations over the U.S.
256 (25°N-55°N) between the precipitation responses of the global and tropical Pacific experiments
257 which are 0.70, 0.77, 0.72 for March, April and May, respectively. There is also considerable
258 similarity between the height anomalies (second column of Fig. 7). This indicates that the
259 tropical Pacific SST anomalies dominate the SST-related precipitation and height responses over
260 North America.

261

The role of initial land conditions over North America (A-D) is shown in the third columns of Figure 6 and Figure 7 for precipitation and 250mb height, respectively. The main impact of the realistic land initialization occurs during April, with a tendency for wet conditions to occur in a line extending from the central plains to the northeast, and dry conditions in the southeast. Given field significance considerations, we cannot rule out the possibility that the indicated precipitation anomalies are themselves insignificant. Nevertheless, the anomalies are consistent with an apparently significant ridge pattern that develops over the eastern United States (Figure 7) during April. Using an extensive ensemble of AGCM simulations, Koster et al. (2014) show that dry (wet) conditions in the south central U.S. tend to produce a large-scale planetary wave pattern that includes a southward (northward) anomaly in the 250-mb meridional wind field in the eastern half of the U.S. and which would be associated with an anomalous low (high) in the 250-mb height field along the East Coast. In our experiments here, soil moisture conditions on 1 March 2011 are characterized by a wet anomaly in the north central U.S. that persists into April; extrapolating somewhat from the Koster et al. (2014) study (and as more directly supported by additional land-focused AGCM experiments, not shown), this could indeed induce a high along the East Coast as part of a broader planetary wave pattern. The pattern would not similarly appear in March given the presence of snow cover as well as a reduction in evaporation anomalies associated with reduced surface radiative forcing. The absence of the pattern in May may reflect the fact that by this time, the initial soil moisture anomaly has weakened (not shown).

283 The last column in Figure 6 shows the joint impact of realistic global atmospheric and land
284 initialization (B-Bc). This column highlights the important contribution of the initial conditions
285 (especially for the atmosphere) to the full precipitation response shown in Figure 4. Indeed,
286 some of the main features (especially the negative anomalies in the eastern U.S.) of the full
287 precipitation response (second column of Figure 4) can be attributed to the initial conditions.
288 Figure 7 (last column) shows that the impact of the initial conditions is associated with large-
289 scale height anomalies, with March showing the signature of a positive NAM and wave-like
290 features extending across North America (with negative anomalies extending southwestward
291 across the continent), the North Atlantic and Europe. The NAM appears to persist into April
292 along with the important negative height anomalies over eastern Canada and the northeastern
293 United States, and positive anomalies to the south. In May the anomalies are quite weak,
294 indicating there is little impact of the initial conditions three months into the predictions.

295

296 The relatively large impact of the initial conditions extending well into April is rather surprising
297 in light of the relatively weak impact of the North American land initial conditions (discussed
298 above) and generally accepted estimates of weather predictability that suggest one should expect
299 little if any skill from atmospheric initial conditions beyond a few weeks (e.g., Lorenz 1969;
300 Chang et al. 2000). In particular, the NAO has been estimated to have an e-folding time of 9.5
301 days (Feldstein 2000). It is possible that the initial atmospheric conditions contain information
302 from prior SST forcing, and this can impact the forecasts several weeks into the future (e.g.,
303 Barsugli et al. 1999; Branstator 2014), though the main height anomalies linked to the initial
304 conditions also suggest a high latitude connection (with a clear NAM component).

An alternative mechanism for extending predictability into the second month involves the dynamical coupling between the stratosphere and troposphere through downward propagation of zonal wind anomalies, through which NAM variability in the lower stratosphere can provide enhanced predictability of tropospheric NAM variability (e.g., Baldwin and Dunkerton 1999). The stratospheric Arctic vortex was unusually cold and persistent during the winter and spring of 2011. Hu and Xia (2013) found that beginning the middle of February the stratospheric NAM showed downward propagation that led to enhancement of the tropospheric NAM, reaching maximum values in late March and April. Karpechko et al. (2014) found in a modeling study of the impact of the 2011 spring Arctic ozone depletion that, while both SST and ozone depletion played a role in producing the downward propagation of the zonal wind anomalies to the troposphere following the strong polar vortex event in late winter and early spring, the magnitude of the event is only captured if preconditioning (likely associated with internal atmospheric dynamics) is reproduced both in the troposphere and lower stratosphere. To the extent our initialized runs capture the relevant tropospheric/stratospheric coupling we can expect to have enhanced tropospheric predictability (extending into April), though the exact mechanisms by which that can produce skillful precipitation predictions over North America is unclear.

Finally, we summarize in Table 2 the similarity between the total precipitation response (second column in Fig. 4) and the separate responses shown in Fig. 6 in terms of the anomaly pattern correlation. The results clearly show the strong impact of the atmospheric conditions during

March, and the importance of the global SST during April and May. It is interesting that the tropical Pacific SST show rather weak correlations despite the greater than 0.7 correlations between the global and Pacific SST responses (mentioned previously). This suggests that subtle phase shifts can have rather large impacts on such a metric and highlights the limitations of using pattern correlations to define similarity. The correlations associated with the North American land response are generally small (even negative during the first month), but increase with lead time though the amplitude of the response is quite weak by May (see our previous discussion of the land impacts for why that might be the case).

3.3 The Intra-Ensemble (Unforced) Component

The differences we see between the ensemble mean results and the reanalysis-based observations, e.g., in terms of U.S. precipitation or height anomalies in the North Atlantic, likely reflect a substantial noise (unforced) component to the anomalies, particularly given that the ensemble mean anomalies tend to be smaller. (We cannot, however, rule out the possibility that the differences reflect deficiencies in the model.) Evidence for large intra-ensemble variance is presented in Figure 8, which shows the height anomalies for individual ensemble members. Of the 44 ensemble members displayed in the figure, only about four achieve the large negative anomalies over eastern North America and the North Atlantic found in the observations. Figure 9 compares one of those four ensemble members with the observed and the ensemble mean. Not only does this member have realistic height anomalies, it also includes the large precipitation anomalies over the Ohio River basin found in the observations. Figure 9 further supports the

348 idea that the observed event has a large random (unforced by SST and land conditions)
349 component.

350

351 To quantify the relative contributions of the SST forced response and the unforced component to
352 the April 2011 height anomalies, we follow the approach of Chang et al. (2012): we reconstruct
353 the MERRA height anomaly field as a linear combination of the model's ensemble mean
354 anomaly and the leading noise components. We compute the noise components based on an
355 REOF decomposition of the April intra-ensemble variance computed from the various model
356 experiments.

357

358 The four leading noise REOFs consist of the NAM, a Northern Eurasian wave mode, the NAO,
359 and the North Pacific Oscillation (NPO). Using the leading RPCs as predictors, it turns out that
360 the NAM (E_1), the NAO (E_3), and the eighth[7] REOF (E_8) provide a minimal set of predictors for
361 the unforced part of the variance, allowing the reproduction (together with the forced response)
362 of the observed height anomalies. In particular, we form the regression equation:

363 $$\Delta_{obs} = \overline{\Delta}_{model} + aE_1 + \beta E_3 + \gamma E_8 + \epsilon, \quad (6)$$

[7] It turns out that the eighth mode is required to reproduce the short wave pattern across the North Pacific. This unforced pattern is very likely unpredictable and the fact that it happens to project on the eighth REOF almost certainly occurs purely by chance. We do not claim that this REOF is in any way statistically distinct.

where ε is a residual and α, β, and γ are the regression parameters. Also, Δ_{obs} is the April 2011 MERRA height anomaly and $\bar{\Delta}_{model}$ is the model's ensemble mean anomaly for that month.

The results of the reconstruction are presented in Figure 10. The left panels show the observed anomalies (top panel), the forced response (ensemble mean, middle panel), and the reconstructed field (bottom panel), the latter consisting of the ensemble mean plus the weighted sum of the first, third and eighth REOFs. The resemblance of the reconstructed field to the observed over the western hemisphere is remarkable.

These results (together with those shown in Figure 2) indicate that the NAO plays a key role in producing the most extreme anomalies over the U.S. during April. We thus turn next to a more detailed analysis of that mode.

3.4 The NAO mode

A key question is whether there was a predilection for an extreme NAO-like mode to develop during April 2011 – particularly whether an SST-forced change in the base state made the development of the NAO more likely than average. Here we turn to experiments with the stationary wave model (SWM) described in section 2. We begin with a look at observations-based experiments designed to establish the leading forcing terms and to assess the ability of the SWM to reproduce the NAO's structure. This is followed by an examination of additional AGCM-based SWM experiments designed to isolate SST-forced changes in the base state during April 2011 that might have increased the likelihood of an extreme NAO event.

385

386 In the first set of experiments, the background state consists of the full three-dimensional March-
387 April-May mean climatological flow computed from MERRA for the period 1980-2011. The
388 stationary wave forcing includes anomalies of diabatic heating, vorticity and temperature
389 transient flux convergences and divergence terms (see Schubert et. al. 2011 for details of the
390 leading forcing terms). In order to isolate the forcing associated with the NAO, we compute the
391 forcing terms at each grid point and for each spring month based on the daily MERRA data for
392 1980-2011. The monthly forcing terms are then regressed against the normalized springtime
393 monthly RPC 3, i.e., the time series of the pattern most resembling the NAO from MERRA.
394 Figure 11 provides an example of two of the leading forcing terms. The heating anomalies in the
395 middle troposphere (top panel) consist of a tripole pattern in the North Atlantic, with heating to
396 the south of Greenland juxtaposed with cooling to the south (located just north of 30°N), and
397 heating over the Caribbean Sea and western tropical North Atlantic. There is also a heating
398 anomaly centered over the central tropical Pacific. The inverse Laplacian[8] of the transient
399 vorticity forcing (bottom panel of Figure 11) also shows a tripole pattern over the North Atlantic
400 extending westward over eastern North America. The North Pacific is characterized by negative
401 anomalies in middle latitudes with positive anomalies to the north extending into the Arctic.

402

403 We now examine the extent to which the MERRA-based NAO anomalies can be reproduced by
404 the SWM when driven by these forcing terms. Figure 12 shows the responses of the

[8] The inverse Laplacian provides a filtered view of what is otherwise a rather noisy field.

streamfunction in the model upper troposphere (σ=0.257) to the leading forcing terms (diabatic heating, temperature transients, and vorticity transients). The response to the transient vorticity flux convergences looks remarkably like the positive NAO streamfunction obtained via regression directly from MERRA (cf. top left and bottom left plots in Figure 12). A key difference is that the negative anomalies over North America and the North Atlantic in MERRA are shifted further east. The response to the temperature transients (bottom right panel of Figure 12) is largely out of phase with the response to the vorticity transients; it is also weaker, so that the combined response still resembles the regressed NAO field, but with reduced amplitude, especially over North America/Greenland. The response to the diabatic heating (middle left panel) is generally weaker than that from the other terms, though it does make substantial contributions to the anomalies over the North Atlantic. Overall we find that the response to the sum of the transients and the diabatic heating (top right panel in Figure 12) does resemble the NAO pattern, though the amplitude is too weak, especially in northern high latitudes (particularly over North America).

A key caveat of the above analysis concerns the nature of the transient eddy forcing. As Feldstein (2003) points out, the NAO is driven by nonlinear processes with the transient eddies playing a key role. While the high frequency transients act in part as a feedback mechanism to prolong the lifecycle of the NAO, the question of what processes organize the transients to drive the NAO in the first place is still not well understood. As such, one must be careful in interpreting the eddies as a forcing term (as we do above), when in fact the existence of the eddies depends at least in part on the existence of the NAO.

427

428 Despite the above limitation, we believe the SWM-based analysis of the forcing of the NAO is
429 sufficiently realistic to allow the use of the SWM for a study of the impact on the NAO of
430 changes in the base state. In particular, we examine whether the anomalous (SST-forced) 3-
431 dimensional April 2011 state was unusually conducive to the development of a large amplitude
432 NAO. We use the same approach as above, but now, instead of using MERRA fields, we
433 compute the forcing terms for April 2011 based on the intra-ensemble variability of the model
434 simulations. The monthly forcing terms are then regressed against the model's normalized April
435 RPC 3, which is the pattern most resembling the NAO from the model simulations. We examine
436 two different April base states: a control consisting of the average of all the ensemble members
437 for the years 2000-2010, and the anomaly base state consisting of the mean of the 2011 ensemble
438 members. The former is our estimate of the model's climatological April base state, while the
439 latter (when differencing it from the control state; A-Ac in Table 1) provides an estimate of how
440 the SST impacted the base state during April 2011 (e.g., Fig. 5a).

441

442 The top left panel of Figure 13 shows the AGCM's NAO stream function pattern (plotted for the
443 positive phase) in the upper troposphere (σ=0.257) computed by linearly regressing the intra-
444 ensemble stream function anomalies against the model's normalized RPC3 values (the associated
445 REOF is shown in the right, middle panel of Figure 10). This is our target for what we expect to
446 reproduce with the SWM. The results of the SWM are shown in the remaining panels. The
447 base state is (as described above) the April 2011 three-dimensional ensemble mean of the
448 AGCM runs. We see that the SWM-generated pattern for all of the forcing terms combined (top

449 right panel of Figure 13) does resemble the AGCM NAO pattern, though it is again somewhat
450 weaker in amplitude. The primary forcing comes from the vorticity transients (middle left
451 panel), with a secondary contribution from the temperature transients (middle right panel; in
452 quadrature with the response to the vorticity transients). Heating provides a negligible
453 contribution (not shown).

454

455 The bottom panel of Figure 13 shows the SWM results obtained with the April 2011 ensemble
456 mean state (shown in the top right panel) minus the results obtained using the control
457 (climatological) April base state. It thus shows the impact of the base state changes in April
458 2011 induced by SST anomalies. A wave number 1 pattern appears at high latitudes in the
459 difference plot, a pattern that acts to enhance the positive NAO (cf. top left panel). Similar
460 results (but with opposite sign) are obtained when the SWM is driven with forcing of the
461 opposite sign, indicating that the results are quite linear. Overall, the SWM-based results
462 indicate that the April 2011 SST anomalies did indeed have some modest influence on the NAO
463 through changes in the base state, acting to produce a predilection for a more intense NAO,
464 though the resulting NAO could have been of either sign.

465

466 We find some support for an enhanced intra-ensemble variance of RPC 3 (the NAO mode
467 computed from experiment A) compared with the climatological value (computed from
468 experiment Ac), though the results are not statistically significant[9]. We note that Karpechko et

[9] Based on a F-test for the ratio of the variances at the 90% significance level.

al. (2014) found that the effect of SST and ozone forcing was to increase the probability of positive NAM events of large magnitude during the spring of 2011, a result that further supports the idea that the high latitudes had a predilection for increased variability. In any event, even if the April 2011 enhanced variance of RPC 3 is real, it would translate to a change in the probability of exceeding the observed value (assuming a normal distribution) from the already climatologically small probability of 0.26% to only 0.85% – still a very small probability.

4. Summary and Conclusions

A series of AGCM simulations were carried out to examine the causes of the extreme weather activity and associated record-breaking precipitation that occurred throughout much of the Ohio River Valley in the spring of 2011. Our analysis focused on April (the month with the most extreme precipitation anomalies) employing a moderately high (¼°) horizontal resolution version of the GEOS-5 AGCM run for the period 1 March through 31 May. Several different ensembles of runs were carried out in an attempt to isolate the role of SST forcing and initial (both atmospheric and land) conditions. The key result of the model simulations is that the record-breaking precipitation that occurred in April is primarily the result of the development of an unusually large amplitude positive NAO-like (free) mode, while it was only weakly forced by SST and land conditions. The direct impact of the SST was primarily to produce drying and warming in the southern plains (with only weak wet anomalies in the northeast), while the impact of realistic initial North American land conditions was a tendency for wet conditions to

491 occur in a line extending from the central plains to the northeast, and dry conditions in the
492 southeast.

493

494 A complicating factor in our assessment of the SST and land impacts is that the initial
495 atmospheric condition[10] was the primary contributor to the April ensemble mean precipitation
496 response in the Ohio River Basin. The source of that signal (which occurs well beyond the range
497 of weather predictability) is unclear. One possibility is that it reflects in the initial conditions the
498 impact of past SST forcing (e.g., Barsugli et. al. 1999; Branstator 2014). Another possibility is
499 that stratospheric/tropospheric coupling played a role. The polar vortex was unusually cold and
500 persistent that winter and spring and there is clear evidence for downward propagation from the
501 stratosphere that led to an enhancement of the tropospheric NAM in March and April (Hu and
502 Xia 2013). Karpechko et al. (2014) further showed that preconditioning (likely associated with
503 internal atmospheric dynamics) played an important role in the downward propagation following
504 the strong polar vortex event (though ozone depletion and SST forcing also played a role). As
505 such, we cannot fully distinguish the contributions of the SST from other potential sources of the
506 signal that might be reflected in the initial conditions.

507

508 The important role of the NAO has major implications for the predictability of the circulation
509 and precipitation anomalies. Figure 14 shows the signal-to-noise ratios of the global upper level

[10] While this is based on runs that also included realistic global land initial conditions, our runs that isolated the role of North American land conditions indicates that the land cannot account for the relatively large April ensemble mean precipitation response.

510 height and U.S. precipitation fields for April 2011 based on hindcasts initialized at the beginning
511 of March (experiment A). While the height field does show ratios larger than 2 over a
512 substantial part of North America (and of course over much of the tropics), the ratios for
513 precipitation over the U.S. are generally quite small (e.g., less than 0.5 over the key region of the
514 Ohio River basin). As mentioned earlier, the NAO is known to have limited predictability at
515 monthly and longer time scales reflecting the intrinsic short time scales of this mode. This is the
516 result of the dynamical processes that govern the growth, maintenance and decay of the NAO -
517 processes that are dominated by transient eddy fluxes (Section 3.4; Feldstein 2003). Our results
518 are consistent with the study by Pegion and Webb (2014), which concluded that the
519 meteorological factors leading to the 2011 flood are not accurately predicted at seasonal lead
520 times by state-of-the-art operational and experimental forecast systems. There is some indication
521 of larger ratios (exceeding 1) in the southwest and along the southern tier of states that are likely
522 linked to La Nina.

523

524 The question of whether there was some predilection for an extreme positive NAO during April
525 2011 was addressed here using an SWM. Our results indicate that the SST-forced (ensemble
526 mean) base state for April 2011 did indeed enhance the amplitude of the NAO response
527 compared to that of the climatological state, though the impact is modest and can be of either
528 sign (contributing to either a positive or negative NAO, depending on the sign of the forcing).
529 Our assessment of whether the April 2011 intra-ensemble variance of the NAO was elevated
530 compared with its climatological value was inconclusive (results were not statistically
531 significant), though even if significant, it would suggest at most only a slight enhancement

(compared to the climatology) of the probability of obtaining a large amplitude NAO during 2011 (still less than 1%).

Acknowledgements: Support for this work was provided by the NASA Modeling, Analysis and Prediction (MAP) Program. We wish to thank the editor, and two anonymous reviewers for their valuable comments that helped to substantially improve the paper.

References

Bacmeister, Julio T., Max J. Suarez, Franklin R. Robertson, 2006: Rain Reevaporation, Boundary Layer–Convection Interactions, and Pacific Rainfall Patterns in an AGCM. *J. Atmos. Sci.*, **63**, 3383–3403. doi: 10.1175/JAS3791.

Baldwin, M. P., and T. J. Dunkerton, 1999: Propagation of the Arctic Oscillation from the stratosphere to the troposphere. J. Geophys. Res.,104, 30937–30946.

Barnston A.G. and R. E. Livezey, 1987: Classification, seasonality, and persistence of low-frequency atmospheric circulation patterns. Mon. Weather Rev. 115, 1083–1126.

Barsugli, J.J., J.S. Whitaker, A.F. Loughe, P.D. Sardeshmukh, and Z. Toth, 1999: The Effect of the 1997/98 El Niño on Individual Large-Scale Weather Events. Bulletin of the American Meteorological Society, Volume 80, Issue 7 (July 1999) pp. 1399-1411.

559 Branstator, G., 2014: Long-Lived Response of the Midlatitude Circulation and Storm
560 Tracks to Pulses of Tropical Heating Journal of Climate, 27, 8809-8826. DOI:
561 http://dx.doi.org/10.1175/JCLI-D-14-00312.1

562

563 Chang, Y., S.D. Schubert and M. J. Suarez, 2000: Boreal winter predictions with the
564 GEOS-2 GCM: The role of boundary forcing and initial conditions. Quart. J. Roy.
565 Met.Soc., 126, 1-29, 2000

566 Chang, Y., S. Schubert and M. Suarez, 2012: Attribution of the Extreme U.S. East Coast
567 Snowstorm Activity of 2010, J. Climate, 25, 3771-3791, 2012..

568

569 Chen, M., P. Xie, and Co-authors, 2008: CPC Unified Gauge-based Analysis of
570 Global Daily Precipitation, Western Pacific Geophysics Meeting, Cairns,
571 Australia, 29 July - 1 August, 2008.

572

573 Collins, N., G. Theurich, C. DeLuca, M. Suarez, A. Trayanov, V. Balaji, P. Li, W.
574 Yang, C. Hill, and A. da Silva, 2005: Design and implementation of
575 components in the Earth System Modeling Framework. *Int. J. High Perf.*
576 *Comput. Appl.*, **19**, 341-350, DOI: 10.1177/1094342005056120.

577

578 Feldstein, S. B., 2000: The timescale, power spectra, and climate noise properties

of teleconnection patterns. *J. Climate*, **13**, 4430–4440.

Feldstein SB. 2003. The Dynamics of NAO teleconnection pattern growth and decay. Q. J. R. Meteorol. Soc. 129 : 901–924.

FEMA 2012: Tornado Outbreak of 2011. Mitigation Assessment Report. FEMA P-908 / May 2012.

Held, I. M., M. Ting, and H. Wang, 2002: Northern winter stationary waves: theory and modeling. *J. Climate*, **15**, 2125-2144.

Hoerling, Martin, Jon Eischeid, Robert Webb, 2013a: Understanding and Explaining Climate Extremes in the Missouri River Basin Associated with the 2011 Flooding. Climate Assessment Report. Prepared for the US Army Corps of Engineers by the National Oceanic, 27 December 2013.

Hoerling, Martin, Arun Kumar, Randall Dole, John W. Nielsen-Gammon, Jon Eischeid, Judith Perlwitz, Xiao-Wei Quan, Tao Zhang, Philip Pegion, and Mingyue Chen,

598 2013b: Anatomy of an Extreme Event. *J. Climate*, 26, 2811–2832. doi:
599 http://dx.doi.org/10.1175/JCLI-D-12-00270.1

600

601 Hu, Y. Y., and Y. Xia, 2013: Extremely cold and persistent stratospheric Arctic vortex in
602 the winter of 2010–2011. Chin. Sci. Bull., 58, 3155 – 3160, doi: 10.1007/s11434-
603 013-5945-5

604

605 Hurwitz, M.M., P.A. Newman, and C.I. Garfinkel (2011). The Arctic vortex in
606 March 2011: a dynamical perspective. Atm. Chem. Phys., 11, 11447-11453,
607 doi:10.5194/acp-11-11447-2011.

608

609 Karl, Tom; O'Lenic, Ed; Brooks, Harold; Spring 2011 U.S. Climate Extremes"
610 2011; NOAA's National Climatic Data Center, Asheville, NC.

611

612 Karpechko, A. Yu., J. Perlwitz, and E. Manzini, 2014: A model study of tropospheric
613 impacts of the Arctic ozone depletion 2011, J. Geophys. Res.Atmos.,119,
614 7999–8014, doi:10.1002/ 2013JD021350

615 Kleist D. T., D. F. Parrish, J. C. Derber, R. Treadon, W.-S. Wu, and S. Lord, 2009:
616 Introduction of the GSI into the NCEPs Global Data Assimilation System. Wea.
617 Forecasting, 24, 1691- 1705.

Koster, R.D., M.J. Suárez, A. Ducharne, M. Stieglitz, and P. Kumar, 2000: A catchment-based approach to modeling land surface processes in a GCM, Part 1, Model Structure. *J. Geophys. Res.*, **105**, 24809- 24822.

Koster, R. D., Y. Chang, and S. D. Schubert, 2014: A mechanism for land-atmosphere feedback involving planetary wave structures. J. Climate, 27, 9290-9301.

Lin, S.-J., 2004: A vertically Lagrangian finite-volume dynamical core for global models. *Mon. Wea. Rev*., **132**, 2293-2307.

Lorenz, E.N., 1969: The predictability of a flow which possesses many scales of motion. Tellus, 21, 289–307, DOI: 10.1111/j.2153-3490.1969.tb00444.x

Molod, A., Takacs, L., Suarez, M., and Bacmeister, J., 2015: Development of the GEOS-5 atmospheric general circulation model: evolution from MERRA to MERRA2, Geosci. Model Dev., 8, 1339-1356, doi:10.5194/gmd-8-1339-2015.

637 Moorthi, S., and M.J. Suarez, 1992: Relaxed Arakawa-Schubert, A
638 Parameterization of Moist Convection for General-Circulation Models.
639 Mon. Wea. Rev. **120**, 978-1002.

640

641 Pegion, K. and R. Webb, 2014: Seasonal Precipitation Forecasts over the Missouri
642 River Basin. An Assessment of Operational and Experimental Forecast
643 System Skill and Reliability. NOAA Report prepared for the Missouri
644 River Basin Water Management Office and the US Army Corps of
645 Engineers. August 2014.

646

647 Pfahl, Stephan and Heini Wernli, 2012: Quantifying the Relevance of Cyclones for
648 Precipitation Extremes. *J. Climate*, **25**, 6770–6780, doi: 10.1175/JCLI-D-11-00705.1.

649

650 Rienecker, M.M., M.J. Suarez, R. Todling, J. Bacmeister, L. Takacs, H.-C. Liu, W.
651 Gu, M. Sienkiewicz, R.D. Koster, R. Gelaro, I. Stajner, and E. Nielsen,
652 2008: *The GEOS-5 Data Assimilation System- Documentation of Versions*
653 *5.0.1, 5.1.0, and 5.2.0*. Technical Report Series on Global Modeling and
654 Data Assimilation, NASA/TM-2007-104606, M.J. Suarez, Ed., Vol. 27, 95
655 pp.

656

Rienecker, Michele M. , Max J. Suarez, Ronald Gelaro, Ricardo Todling, Julio Bacmeister,Emily Liu, Michael G. Bosilovich, Siegfried D. Schubert, Lawrence Takacs, Gi-Kong Kim, Stephen Bloom, Junye Chen, Douglas Collins, Austin Conaty, Arlindo da Silva, Wei Gu, Joanna Joiner, Randal D. Koster, Robert Lucchesi, Andrea Molod, Tommy Owens, Steven Pawson, Philip Pegion, Christopher R. Redder, Rolf Reichle, Franklin R. Robertson, Albert G. Ruddick, Meta Sienkiewicz, and Jack Woollen, 2011: MERRA: NASA's Modern-Era Retrospective Analysis for Research and Applications. *J. Climate*, **24**, 3624–3648. doi: http://dx.doi.org/10.1175/JCLI-D-11-00015.1

Richman M.B., 1986. Rotation of principal components. J. Climatol., 6, 293–335.

Schubert, S., H. Wang, and M. Suarez, 2011: Warm Season Subseasonal Variability and Climate Extremes in the Northern Hemisphere: The Role of Stationary Rossby Waves, J. Climate, 24, 4773-4792, 2011.

Seager, R., L. Goddard, J. Nakamura, N. Henderson, D. E. Lee, 2014: Dynamical causes of the 2010/11 Texas-northern Mexico drought. J. Hydrometeor. 2013, 15, 39-68.

677 Shepherd, M., D. Niyogi, and T. Mote, 2009: A seasonal-scale climatological analysis
678 correlating spring tornado activity with antecedent fall-winter drought in the
679 Southeastern United States, Env. Res. Lett., 4, 24012, doi:10.1088/1748-
680 9326/4/2/0240
681
682 Ting, M. and L. Yu, 1998: Steady response to tropical heating in wavy linear and
683 nonlinear baroclinic models. *J. Atmos. Sci.,* **55**, 3565–3582.
684
685 Wang, H., S. Schubert, R, Koster, Y.-G. Ham, and M. Suarez, 2014: On the Role of SST
686 Forcing in the 2011 and 2012 Extreme U.S. Heat and Drought: A Study in
687 Contrasts. J. Hydrometeor, **15**, 1255–1273.
688
689 Wu, W.-S., R.J. Purser and D.F. Parrish, 2002: Three-dimensional variational analysis
690 with spatially inhomogeneous covariances. Mon. Wea. Rev., 130, 2905-2916.
691

692 **Table 1**. Here we list the complete suite of GEOS-5 AGCM hindcast experiments. Each
693 set of runs consists of 22 ensemble members, except A which has 44 members, and Ac
694 which has 66 members (6 for each year times 11 years). All model simulations were
695 done at a horizontal resolution of ¼° latitude/longitude. Perturbations (only to the
696 atmosphere) for the runs were produced as: +/- (x-y)/8, where x and y are 2 atmospheric
697 states separated by 1 day, and where the states were obtained from a one month
698 simulation starting in Nov 1. The impacts of the SST and ICs are determined from the
699 runs as follows: both SST and ICs = A – Ac; global SST = A – B; tropical Pacific SST =
700 C – B; atmosphere and land ICs = B – Bc; land ICs over North America = A – D.

Initial Conditions: 1 March, 2011	**Initial Conditions**: 1 March, 2000-2010	**SST**
A	Ac	Observed
B	Bc	climatology (2000-2010)
C		climatology + TPac (2011): (east of 180°; 20°S to 30°N)
D Land initial conditions in the region (130°W-60°W; 35°N-70°N) taken from the years 2000-2010.		2011 Observed

701

Table 2. Anomaly pattern correlations over the continental U.S. (25°N-55°N) between the total ensemble mean precipitation response (A-Ac, second column in Figure 4) and the responses to the individual contributions shown in Figure 6: global SST = A – B, tropical Pacific SST = C – B, land ICs over North America = A – D, and atmosphere and land ICs = B – Bc.

	Global SST	**Tropical Pacific SST**	**N. America Land ICs**	**Global Atmospheric and Land ICs**
March	0.32	0.23	-0.18	0.74
April	0.69	0.33	0.24	0.25
May	0.54	0.15	0.36	0.19

List of Figures

Figure 1: April 2011 anomalies with respect to the climatology spanning the years 2000-2010 of z250mb (meters, top left panel), precipitation (mm/day, shaded) and 850mb moisture flux (g/kg m/s, vectors) anomalies (top right panel), u250mb climatology (5m/s contours) and anomalies (m/s, shaded) (bottom left), and v'^2 250mb anomalies $(m/s)^2$ (bottom right). All fields are from MERRA except the precipitation which is from the CPC unified gauge-based analysis of daily precipitation over CONUS at 0.25° latitude/longitude resolution.

Figure 2: Top left panel: REOF 3 spatial pattern. Bottom left panel: the monthly time series of RPC3 for MAM of each year. Panels on the right show composites based on the extremes (1.5 standard deviations) of RPC3 (positive – negative composites): The top right panel: precipitation (mm/day) and 850mb q fluxes (g/kg m/s). The bottom right panel: v'^2 $(m/s)^2$ at 200mb. The results are for MAM for the period 1979-2012. All fields are from MERRA except the precipitation which is from the CPC unified gauge-based analysis of daily precipitation over CONUS at 0.25° latitude/longitude resolution.

Figure 3: March through May monthly mean SST anomalies (°C) computed with respect to a climatology spanning the years 2000-2010.

730 Figure 4: Left two columns: precipitation anomalies (mm/day) with respect to a climatology
731 spanning the years 2000-2010 from the 0.25° CPC unified gauge-based analysis of daily
732 precipitation, and the ensemble mean of the model simulations (A-Ac: see Table 1) for March
733 –May 2011. Third and fourth columns: same as left two columns but for T2m (°C), and the
734 observed values are from MERRA.

735

736 Figure 5: Ensemble mean results for April 2011 (A-Ac: see Table 1). Top panel: 250mb
737 height anomalies (m). Bottom panel: 250mb v'^2 anomalies $(m/s)^2$.

738

739 Figure 6: Precipitation anomalies (mm/day). Left column: impact of global SST (A-B: see
740 Table 1) for March –May 2011. Second from left column: impact of tropical Pacific SST (C-
741 B). Third column from left: impact of the initial North American (130°W-60°W; 35°N-70°N)
742 land conditions (A-D). Fourth column: impact of global land and atmospheric initial
743 conditions (B-Bc). Contouring indicates values are significant at 90% based on a t-test.

744

745 Figure 7: Same as Fig. 6, except for the anomalies in the 250mb height field (Northern
746 Hemisphere). Units are m.

747

748 Figure 8: April 2011 250mb height anomalies (A-Ac, Table 1) for the 44 individual
749 ensemble members and the observed. Red solid lines outline cases that show a

750 qualitative resemblance to the observed over North America and the North Atlantic
751 (observed is outlined in red dashed line on bottom right) Units: meters.

752

753 Figure 9: Top panels: April 2011 250mb height anomalies (m) with respect to the climatology
754 spanning the years 2000-2010. Bottom panels: same as top panels but for precipitation
755 anomalies (mm/day). Left panels for the ensemble mean (A-Ac). Middle panels: a single
756 ensemble member chosen because of its resemblance to observations. The right panels show
757 the results based on observations: the height anomalies are from MERRA, and the precipitation
758 anomalies are from the CPC unified gauge-based 0.25° analysis of daily precipitation.

759

760 Figure 10: Top left panel: The April 2011 250mb height anomaly with respect to the
761 climatology spanning the years 2000-2010 from MERRA. Middle left panel: the
762 ensemble mean anomaly of the AGCM simulations (A-Ac). Bottom left panel: the
763 reconstructed field based on the ensemble mean and the leading REOFs of April
764 z250mb model intra-ensemble variance (REOFs 1, 3 and 8, shown in the right panels).

765

766 Figure 11: The forcing anomalies obtained from MERRA by regressing the March-
767 April-May monthly interannual anomalies over the period 1980-2011 against the NAO
768 mode (RPC 3). Top panel: mid tropospheric heating. Bottom panel: inverse Laplacian
769 of the transient vorticity term. Values correspond to 1 standard deviation in RPC 3.

770

771 Figure 12: Eddy stream function patterns at sigma=0.257 based on various regressions
772 against the MERRA-based RPC 3 (see Fig. 2) using the March-April-May monthly
773 anomalies over the period 1980-2011. Top left panel: the regressed NAO pattern
774 plotted for the positive phase. The remaining panels are the responses to the various
775 forcing terms obtained by regressing the forcing against RPC 3. The forcing terms
776 consist of the heating and total transients (top right panel), the heating (middle left
777 panel), the total transients (middle right panel), the vorticity transients (bottom left
778 panel), and the temperature transients (bottom right panel). All values correspond to
779 one standard deviation in RPC 3.

780

781 Figure 13: SWM diagnosis of the NAO for April 2011 based on AGCM results: Top
782 left panel: The AGCM's NAO stream function pattern (plotted for the positive phase)
783 at sigma=0.257, computed by linearly regressing the intra-ensemble stream function
784 anomalies against the model's normalized RPC3 values. The remaining three upper
785 panels show the results from a SWM at sigma level 0.257 in which the forcing
786 associated with NAO was obtained by linearly regressing the intra-ensemble forcing
787 against the normalized RPC3 values. The base state is the April 2011 three-
788 dimensional ensemble mean of the AGCM runs. Top right panel: the results for all
789 three forcing terms (vorticity and temperature transients, and heating). Middle left
790 panel: the results when the SWM was forced with just the vorticity transients. Middle
791 right panel: the results for just the temperature transients. Bottom panel: the SWM
792 results obtained with the April 2011 ensemble mean state (shown in top right panel)

793 minus the results obtained using a climatological April base state computed from the
794 AGCM runs spanning 2000-2010.

795

796 Figure 14: The square of the ensemble mean anomaly divided by the intraensemble
797 variance for April 2011 (based on 44 ensemble members, experiment A), red contour
798 indicates signal/noise = 1. Top panel is for 250mb height. Bottom panel is for
799 precipitation.

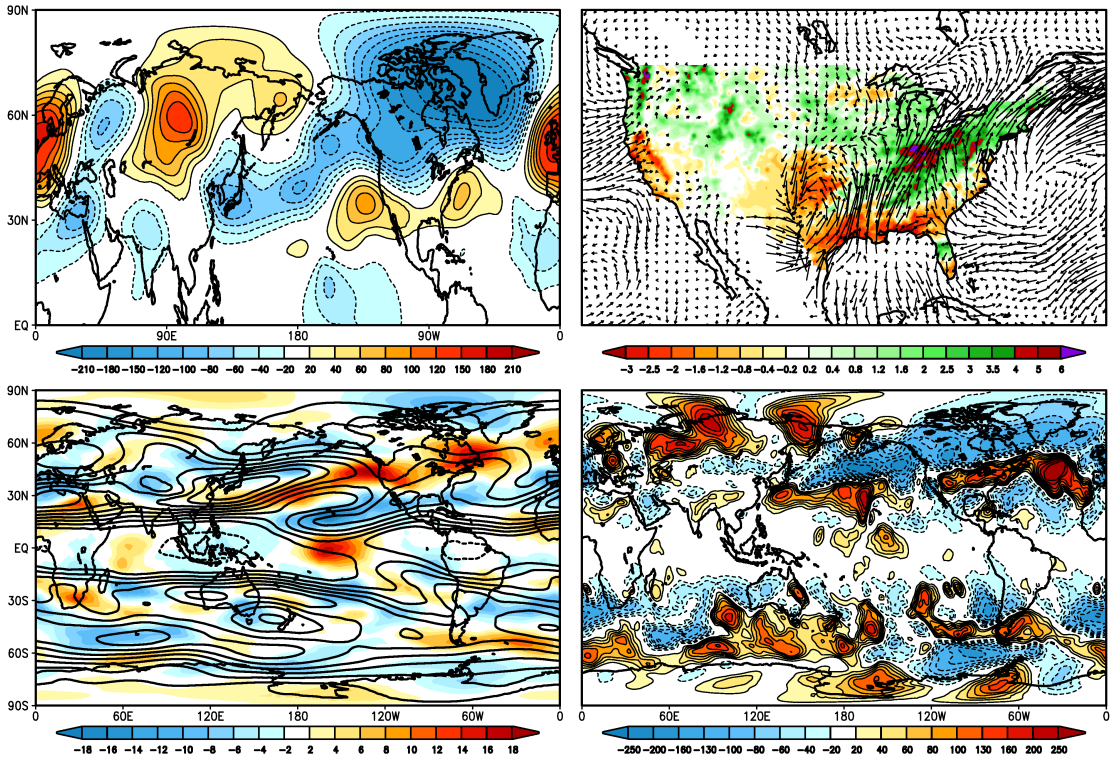

800

801 Figure 1: April 2011 anomalies with respect to the climatology spanning the years

802 2000-2010 of z250mb (meters, top left panel), precipitation (mm/day, shaded) and

803 850mb moisture flux (g/kg m/s, vectors) anomalies (top right panel), u250mb

804 climatology (5m/s contours) and anomalies (m/s, shaded) (bottom left), and v'^2 250mb

805 anomalies $(m/s)^2$ (bottom right). All fields are from MERRA except the precipitation

806 which is from the CPC unified gauge-based analysis of daily precipitation over

807 CONUS at 0.25° latitude/longitude resolution.

808

809

810

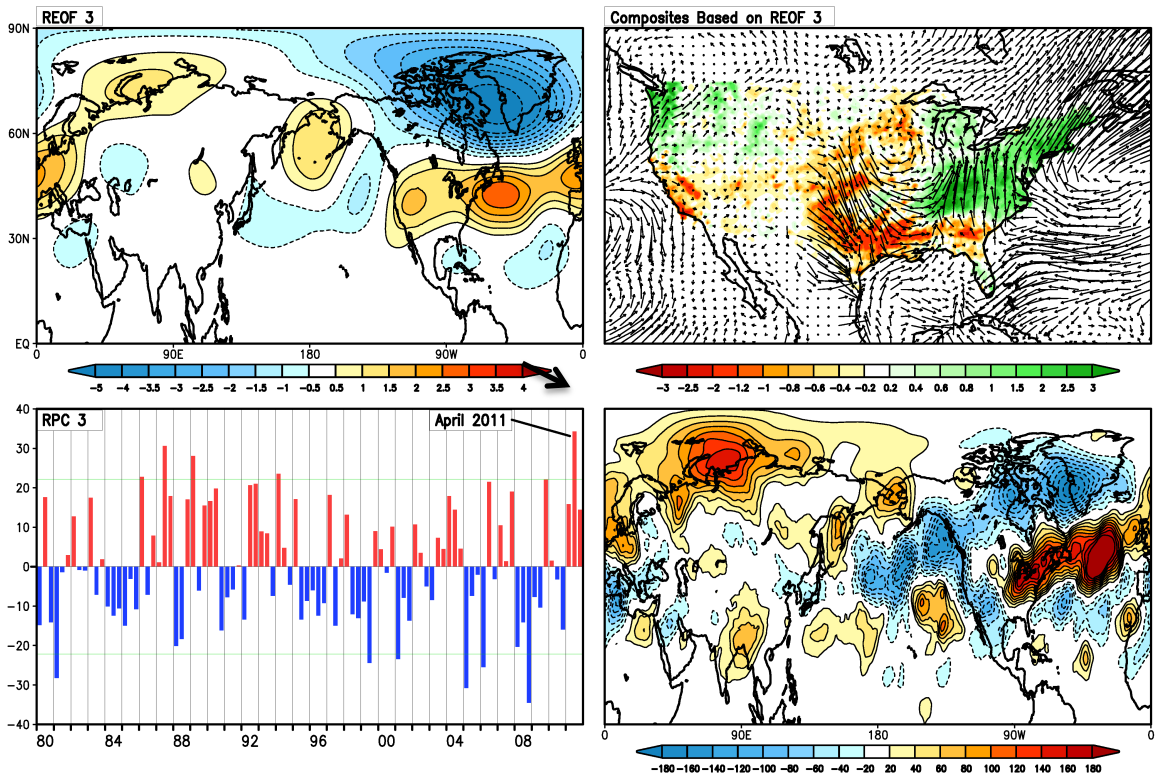

811

812 Figure 2: Top left panel: REOF 3 spatial pattern. Bottom left panel: the monthly time

813 series of RPC3 for MAM of each year. Panels on the right show composites based on

814 the extremes (1.5 standard deviations) of RPC3 (positive – negative composites): The

815 top right panel: precipitation (mm/day) and 850mb q fluxes (g/kg m/s). The bottom

816 right panel: v'^2 $(m/s)^2$ at 200mb. The results are for MAM for the period 1979-2012.

817 All fields are from MERRA except the precipitation which is from the CPC unified

818 gauge-based analysis of daily precipitation over CONUS at 0.25° latitude/longitude

819 resolution.

820

821

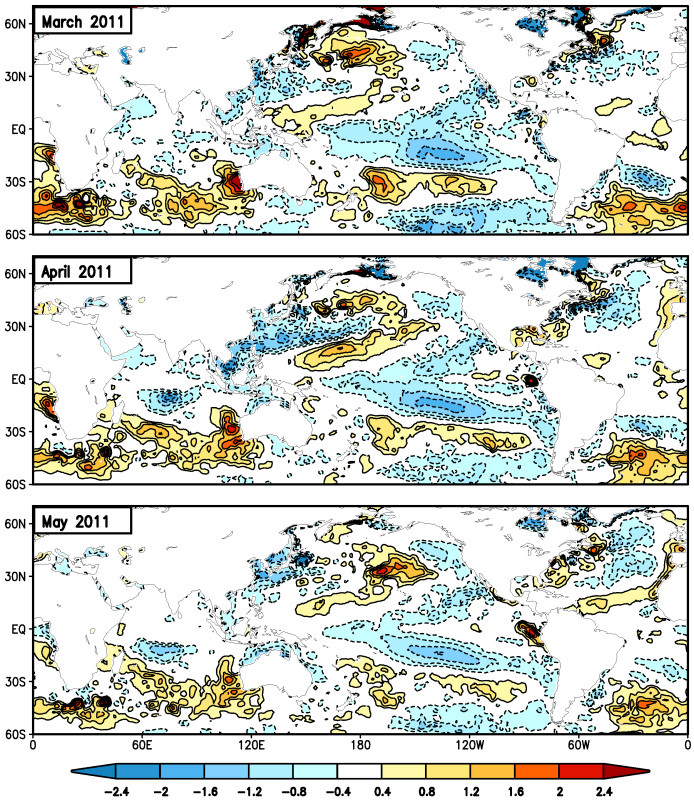

822

823 Figure 3: March through May monthly mean SST anomalies (°C) computed with respect to a

824 climatology spanning the years 2000-2010.

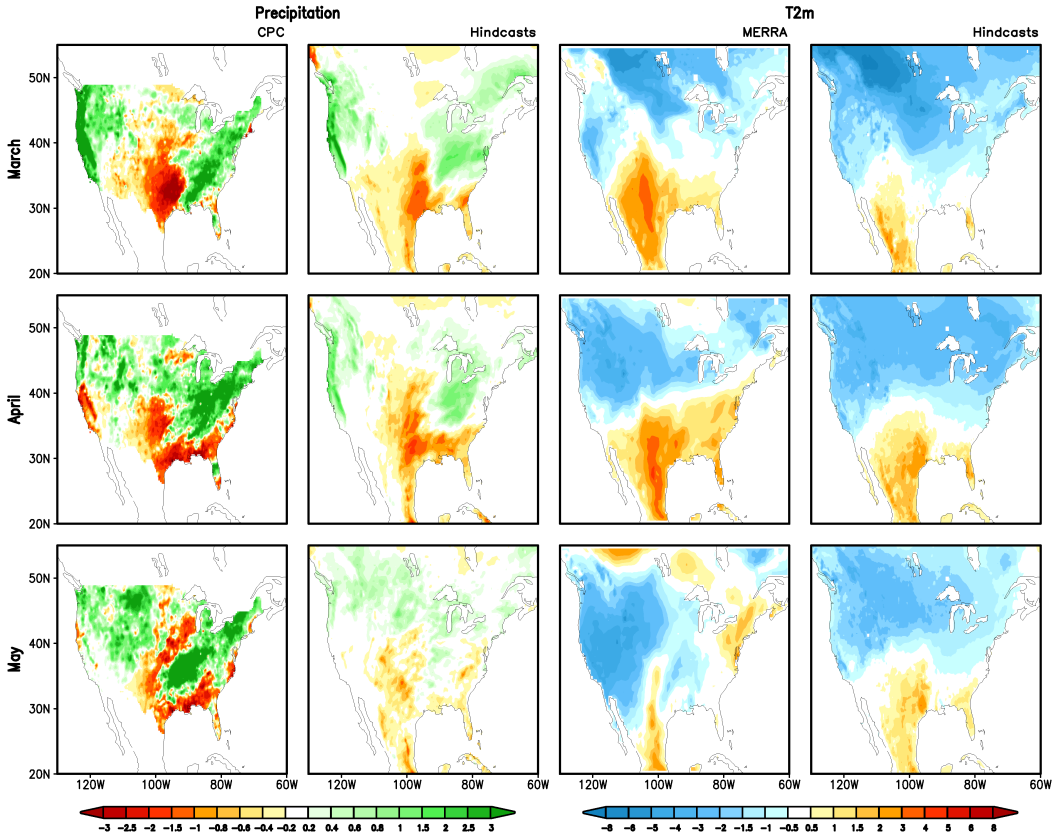

825

826 Figure 4: Left two columns: precipitation anomalies (mm/day) with respect to a climatology
827 spanning the years 2000-2010 from the 0.25° CPC unified gauge-based analysis of daily
828 precipitation, and the ensemble mean of the model simulations (A-Ac: see Table 1) for March
829 –May 2011. Third and fourth columns: same as left two columns but for T2m (°C), and the
830 observed values are from MERRA.

831

832

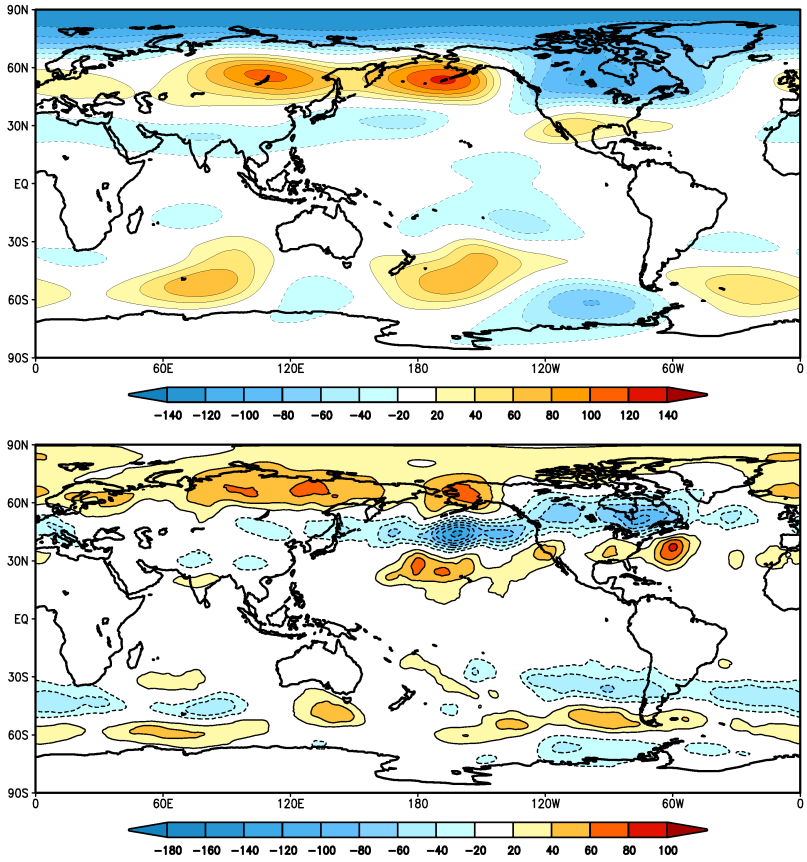

833

834 Figure 5: Ensemble mean results for April 2011 (A-Ac: see Table 1). Top panel: 250mb

835 height anomalies (m). Bottom panel: 250mb v'^2 anomalies $(m/s)^2$.

836

837

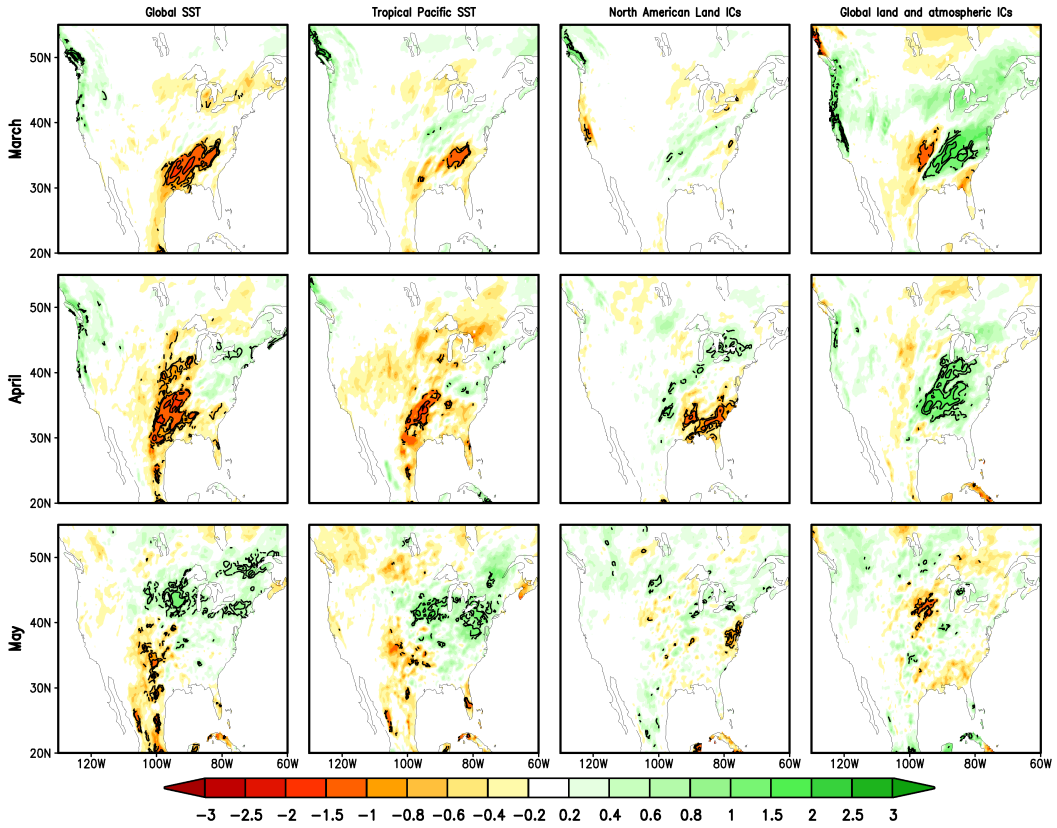

838

839 Figure 6: Precipitation anomalies (mm/day). Left column: impact of global SST (A-B: see
840 Table 1) for March –May 2011. Second from left column: impact of tropical Pacific SST (C-
841 B). Third column from left: impact of the initial North American (130°W-60°W; 35°N-70°N)
842 land conditions (A-D). Fourth column: impact of global land and atmospheric initial
843 conditions (B-Bc). Contouring indicates values are significant at 90% based on a t-test.

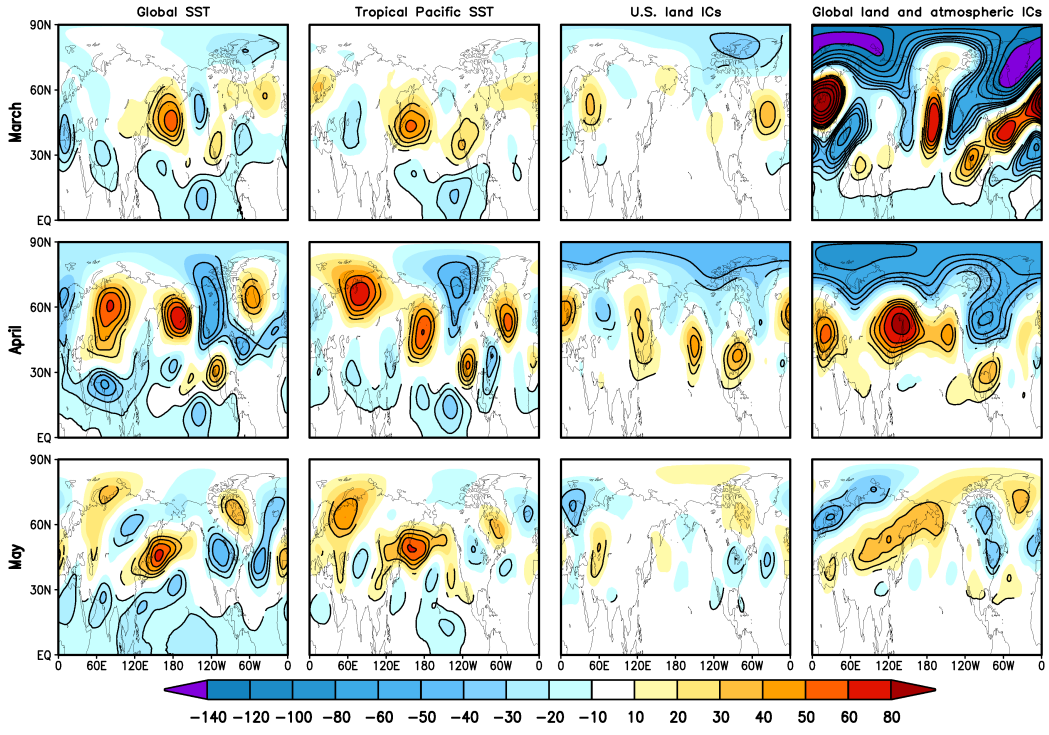

844

845 Figure 7: Same as Fig. 6, except for the anomalies in the 250mb height field (Northern

846 Hemisphere). Units are m.

847

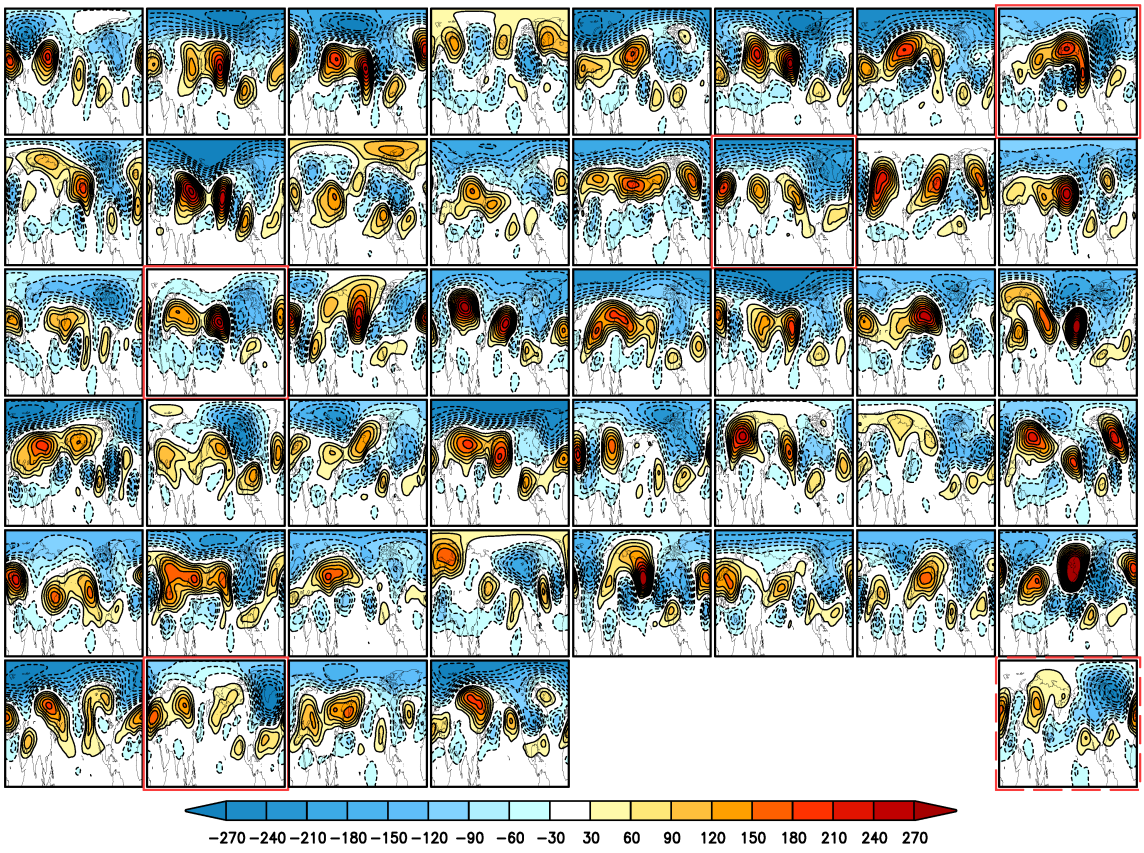

Figure 8: April 2011 250mb height anomalies (A-Ac, Table 1) for the 44 individual ensemble members and the observed. Red solid lines outline cases that show a qualitative resemblance to the observed over North America and the North Atlantic (observed is outlined in red dashed line on bottom right) Units: meters.

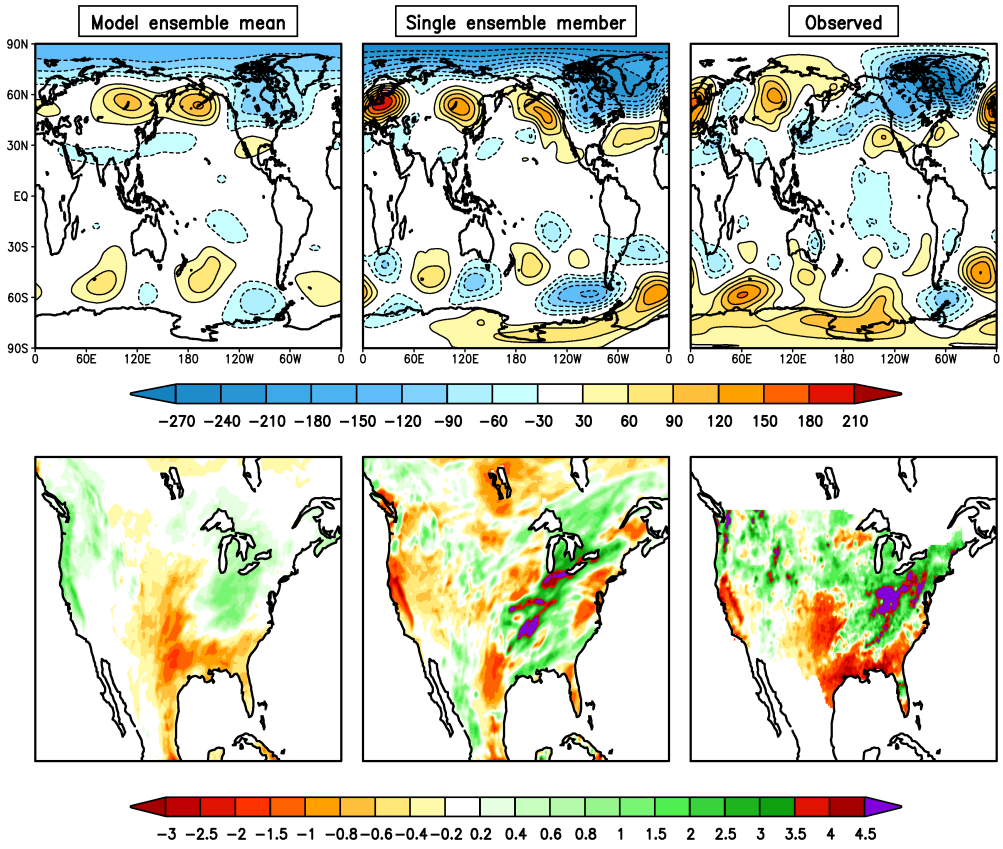

853

854 Figure 9: Top panels: April 2011 250mb height anomalies (m) with respect to the climatology
855 spanning the years 2000-2010. Bottom panels: same as top panels but for precipitation
856 anomalies (mm/day). Left panels for the ensemble mean (A-Ac). Middle panels: a single
857 ensemble member chosen because of its resemblance to observations. The right panels show
858 the results based on observations: the height anomalies are from MERRA, and the precipitation
859 anomalies are from the CPC unified gauge-based 0.25° analysis of daily precipitation.

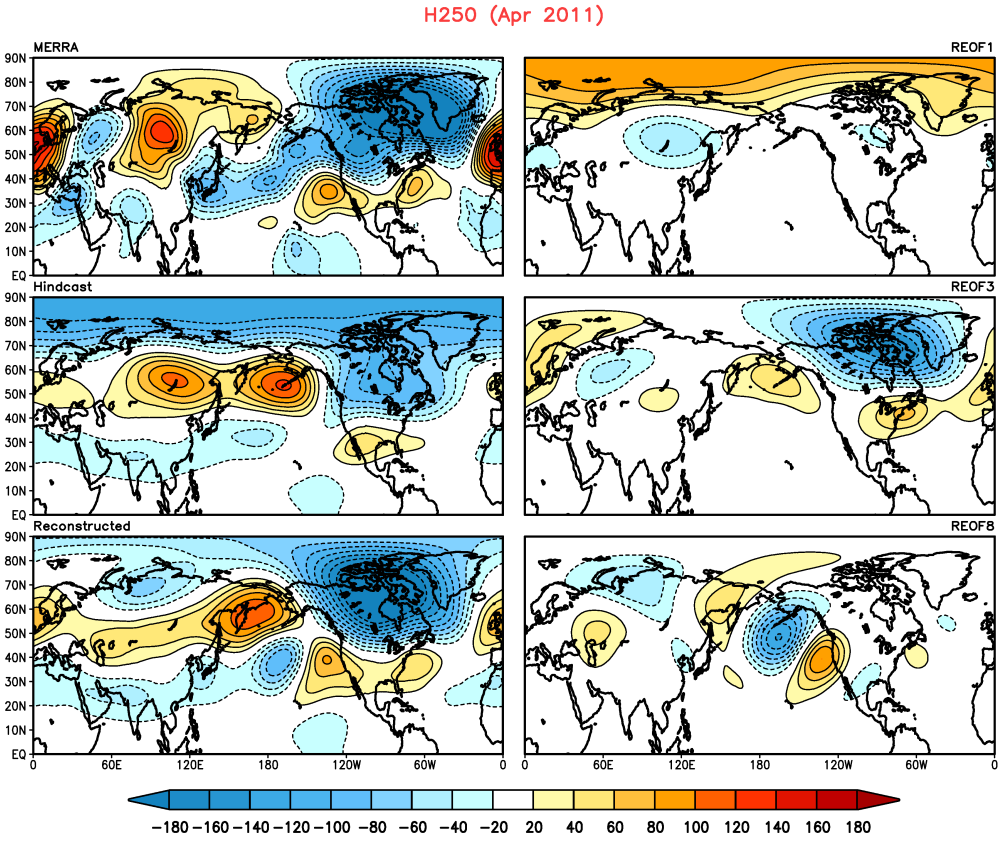

860

861 Figure 10: Top left panel: The April 2011 250mb height anomaly with respect to the
862 climatology spanning the years 2000-2010 from MERRA. Middle left panel: the ensemble
863 mean anomaly of the AGCM simulations (A-Ac). Bottom left panel: the reconstructed field
864 based on the ensemble mean and the leading REOFs of April z250mb model intra-ensemble
865 variance (REOFs 1, 3 and 8, shown in the right panels).

866

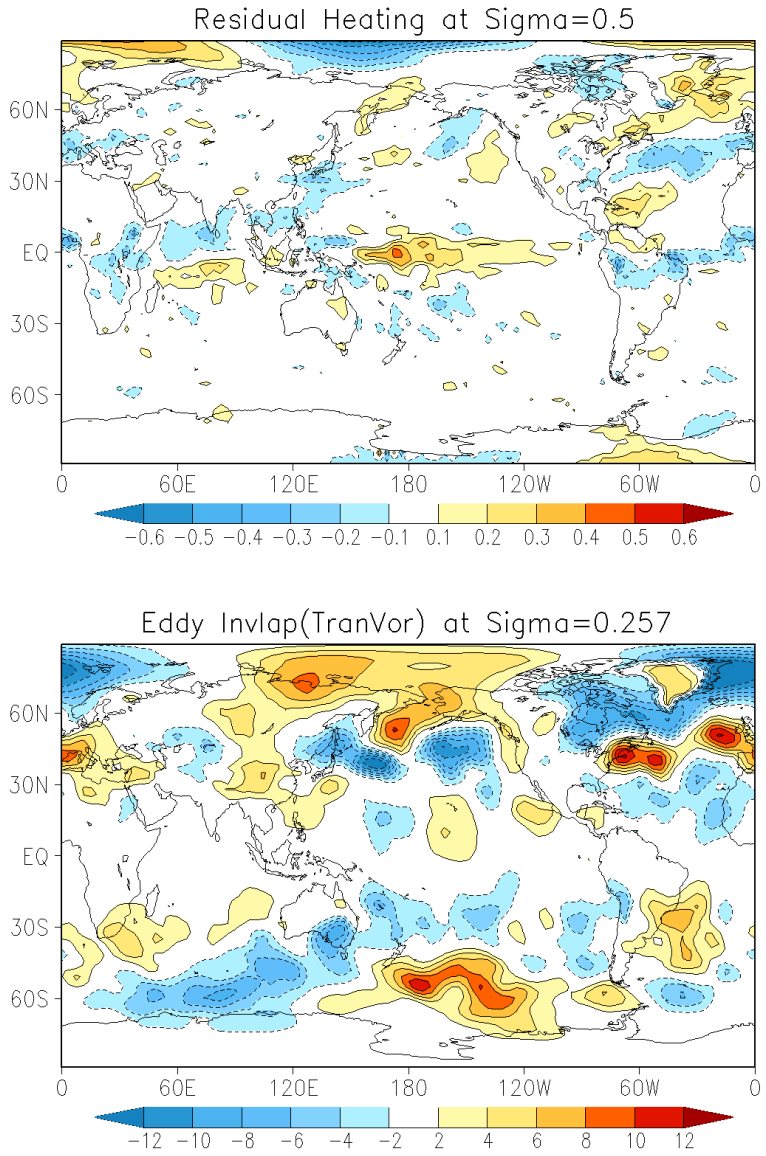

Figure 11: The stationary wave forcing anomalies obtained from MERRA by regressing their March-April-May monthly interannual anomalies over the period 1980-2011 against the NAO mode (RPC 3). Top panel: heating in the middle troposphere (σ=0.5). Bottom panel: inverse Laplacian of the transient vorticity term in the upper troposphere (σ=0.257). Values correspond to 1 standard deviation in RPC 3.

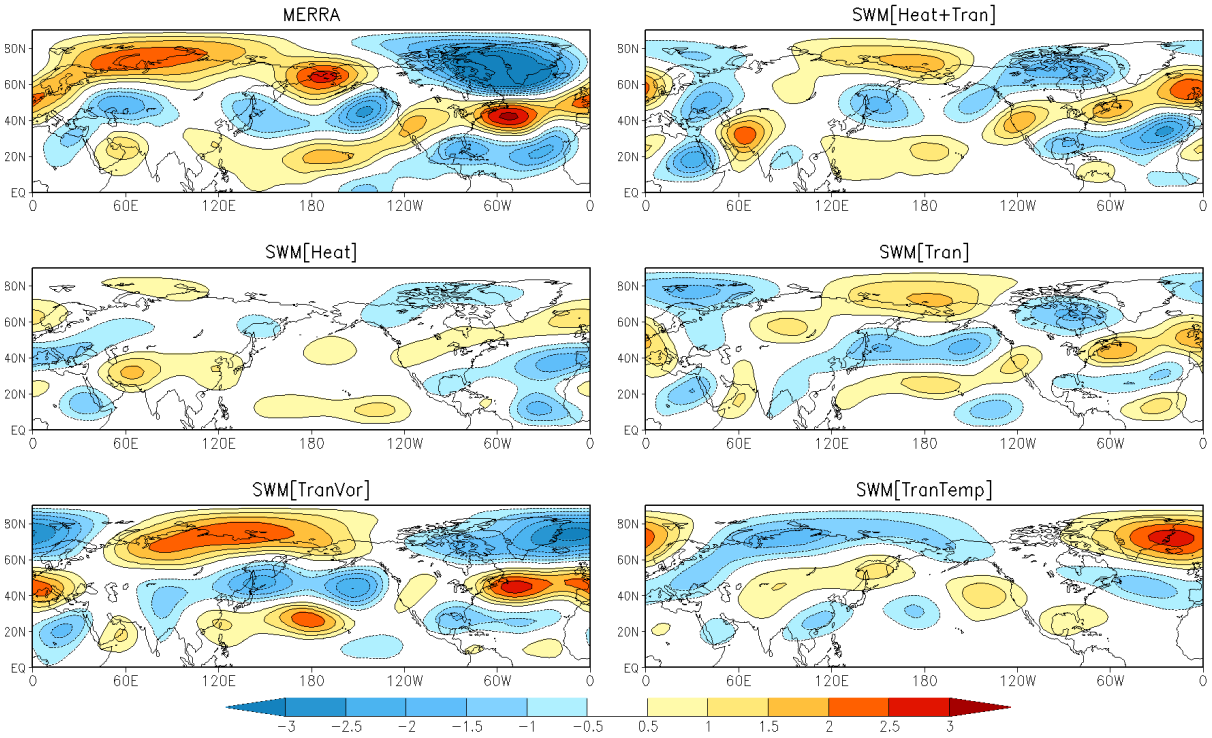

Figure 12: Eddy stream function patterns at σ=0.257 based on various regressions against the MERRA-based RPC 3 (see Fig. 2) using the March-April-May monthly anomalies over the period 1980-2011. Top left panel: the regressed NAO pattern plotted for the positive phase. The remaining panels are the SWM responses to the various forcing terms obtained by regressing the forcing against RPC 3. The forcing terms consist of the heating and total transients (top right panel), the heating (middle left panel), the total transients (middle right panel), the vorticity transients (bottom left panel), and the temperature transients (bottom right panel). All values correspond to one standard deviation in RPC 3.

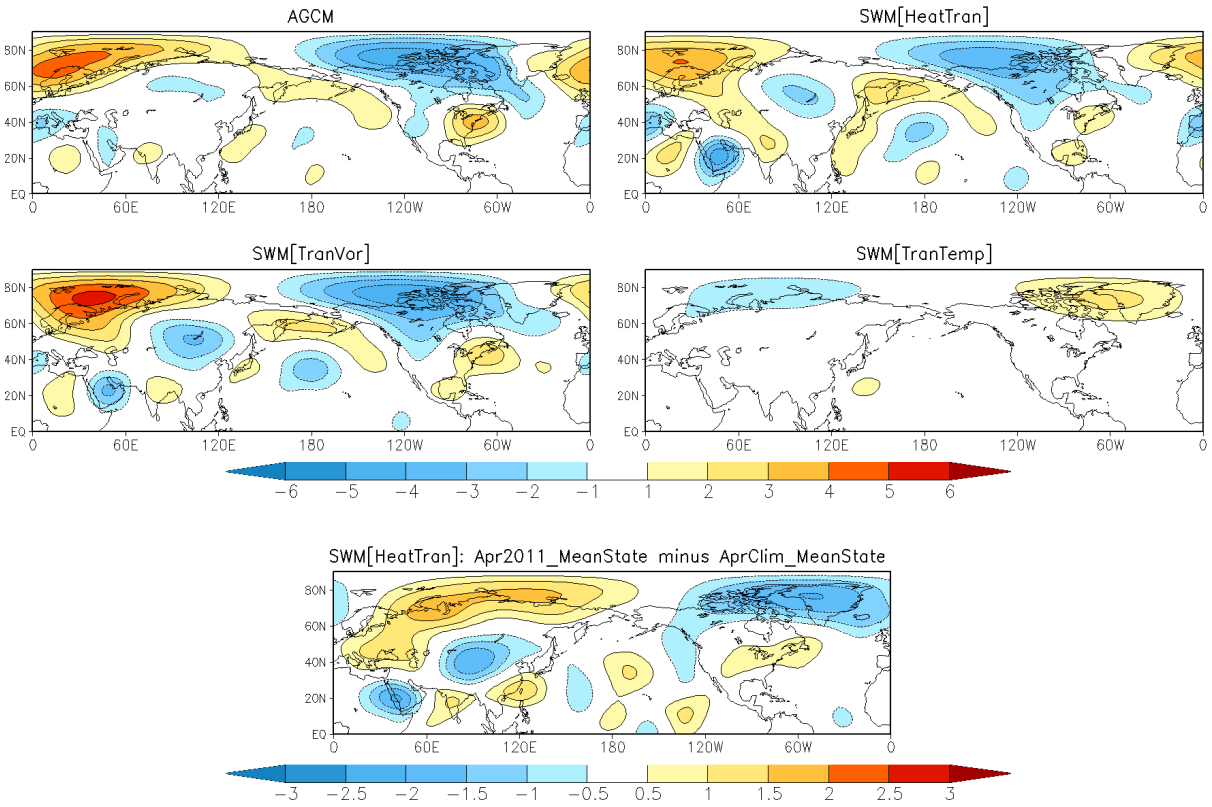

884

885 Figure 13: SWM diagnosis of the NAO for April 2011 based on AGCM results: Top left
886 panel: The AGCM's NAO stream function pattern (plotted for the positive phase) at σ=0.257,
887 computed by linearly regressing the intra-ensemble stream function anomalies against the
888 model's normalized RPC3 values. The remaining three upper panels show the results from a
889 SWM at σ=0.257 in which the forcing associated with NAO was obtained by linearly
890 regressing the intra-ensemble forcing against the normalized RPC3 values. The base state is
891 the April 2011 three-dimensional ensemble mean of the AGCM runs. Top right panel: the
892 results for all three forcing terms (vorticity and temperature transients, and heating). Middle
893 left panel: the results when the SWM was forced with just the vorticity transients. Middle right
894 panel: the results for just the temperature transients. Bottom panel: the SWM results obtained

with the April 2011 ensemble mean state (shown in top right panel) minus the results obtained using a climatological April base state computed from the AGCM runs spanning 2000-2010.

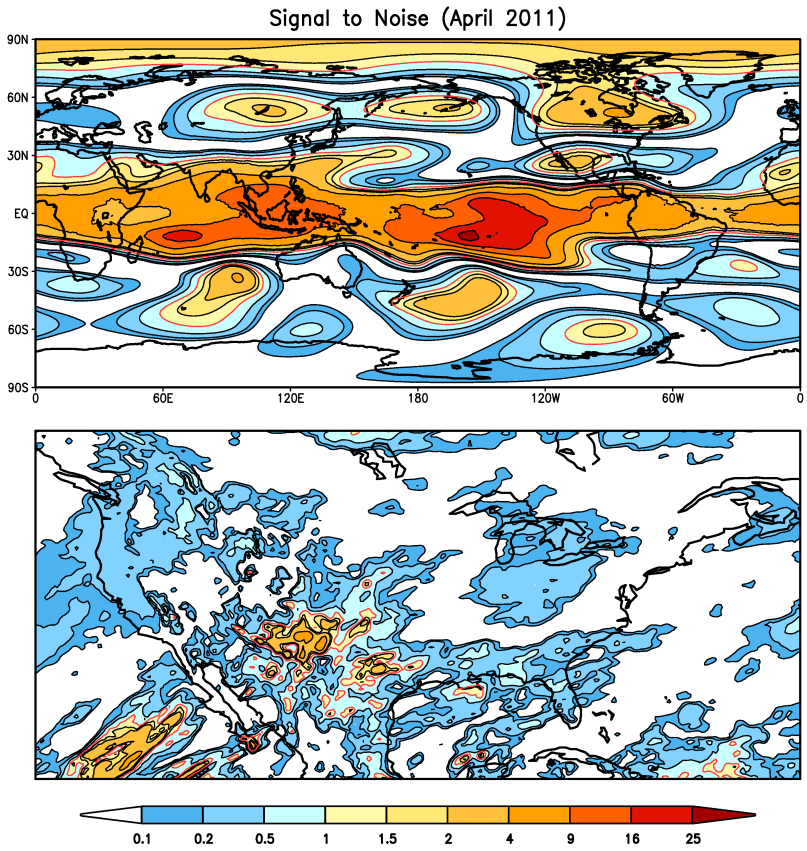

Figure 14: The square of the ensemble mean anomaly divided by the intraensemble variance for April 2011 (based on 44 ensemble members, experiment A), red contour indicates signal/noise = 1. Top panel is for 250mb height. Bottom panel is for precipitation.